arXiv:1601.07517v1 [cond-mat.supr-con] 27 Jan 2016

Ferro-lattice-distortions and charge fluctuations in superconducting $LaO_{1-x}F_xBiS_2$

A. Athauda[1], C. Hoffman[2], Y. Ren[3], S. Aswartham[4], J. Terzic[4], G. Cao[4], X. Zhu[4,5], and D. Louca*[1]

[1]*Department of Physics, University of Virginia, Charlottesville, VA 22904, USA.*
[2]*Oak Ridge National Laboratory, Oak Ridge, TN 37831, USA.*
[3]*Argonne National Laboratory, Lemont, IL 60439, USA.*
[4]*Department of Physics and Astronomy, University of Kentucky, Lexington,KY 40506, USA.*
[5]*Hefei High Magnetic Field Laboratory, Chinese Academy of Sciences, Hefei, China*

January 28, 2016

Abstract

Competing ferroelectric and charge density wave phases have been proposed to be present in the electron-phonon coupled $LaO_{1-x}F_xBiS_2$ superconductor. The lattice instability arises from unstable phonon modes that can break the crystal symmetry. Upon examination of the crystal structure using single crystal diffraction, we find a superlattice pattern arising from coherent in-plane displacements of the sulfur atoms in the BiS_2 superconducting planes. The distortions morph into coordinated ferro-distortive patterns, challenging previous symmetry suggestions including the possible presence of unstable antiferro-distortive patterns. The ferro-distortive pattern remains in the superconducting state, but with the displacements diminished in magnitude. Moreover, the sulfur displacements can exist in several polytypes stacked along the c-axis. Charge carriers can get trapped in the lattice deformations reducing the effective number of carriers available for pairing.

*Corresponding author, louca@virginia.edu

A new class of phonon-mediated superconductors based on BiS_2 layers was recently discovered [1, 2]. The structural features leading to a proposed lattice instability are key to understand the electron-phonon coupling mechanism, a central issue in the superconducting $LaO_{1-x}F_xBiS_2$ [1, 3, 4, 5] of interest in our study. The quasi two-dimensional crystal structure with the superconducting BiS_2 bi-layers sandwiched between insulating LaO layers (Fig. 1A) is reminiscent of the cuprate [6] and iron based superconductors. The Bi atoms form square pyramidal units with in-plane sulfur S1 and apical S2 atoms. First-principles, band structure and spin polarization calculations indicated that a phonon instability breaks the nominal tetragonal symmetry, *P4/nmm*, where the atomic distortions are described using symmetries such as $P2_1mn$ [4], non-centrosymmetric C_2 or the centrosymmetric $P2_1/m$ [7]. Such a change in the crystal symmetry will have significant implications on the band structure thus an experimental verification is necessary.

The Fermi surface is dominated by the hybridized orbitals of Bi $6p$ and S $3p$. Upon fluorine doping via the substitution of oxygen in the insulating layer, as in $LaO_{1-x}F_xBiS_2$, electron carriers are introduced in the lattice [8] and the density of states at the Fermi level increases [3] while the nominal symmetry remains unchanged. Theoretical works [4, 5, 9] suggested that a large phonon softening occurs due to dynamic sulfur displacements, leading to an instability around the Γ point in x = 0, and along Q = (π,π,0) with doping, that has been associated with strong Fermi surface nesting. Earlier neutron powder diffraction measurements showed that indeed sulfur is displaced from its equilibrium position [10], consistent with theoretical predictions, and can possibly lead to charge fluctuations, similar to the parent compound of another phonon superconductor, $BaBiO_3$ [11]. However, to obtain the three-dimensional arrangement of the atomic distortions and possible symmetry breaking conditions, high-resolution single crystal diffraction is clearly needed. To this end, synchrotron X-ray and neutron experiments were carried out on single crystals of $LaOBiS_2$ and superconducting $LaO_{0.7}F_{0.3}BiS_2$ with a T_C of $\sim$2.5 K.

The single crystals were grown using the CsCl/KCl flux method and SEM/EDX was used to determine their stoichiometry, while the bulk magnetization measurements were carried out using a SQUID magnetometer. The synchrotron X-ray experiments on $LaOBiS_2$ and $LaO_{0.7}F_{0.3}BiS_2$ were performed at 11-ID-C using X-rays of 105 KeV at the Advanced Photon Source at Argonne National Laboratory. The data were collected at a wavelength of 0.11798 Å in transmission mode. The neutron scattering experiments were carried out at the single crystal diffractometer TOPAZ at Oak Ridge National Laboratory. The neutron data were background subtracted and corrected for absorption, neutron path length, spectrum, detector efficiency and Lorentz factor. The $LaO_{0.7}F_{0.3}BiS_2$ crystal showed single Bragg peaks at each *hkl* site. The parent compound however showed several Bragg spots at each *hkl* site indicating several grains. In this case, attention was paid to include in the refinement Bragg peaks from the same grain only by calculating the diffraction condition at each Bragg point. The integrated Bragg intensities were determined using the 3D spherical Q space integration and data refinement were performed using the ShelX software [12].

The BiS_2 planes are buckled with equal bond lengths between Bi and S1 at 2.874 Å in the *P4/nmm symmetry* [2, 13, 14, 15, 16, 17] while the bonding between the Bi ion and the apical S2 is shorter, at 2.466 Å, as shown in Fig. 1A. The neutron diffraction pattern shown in Fig. 1B with the Bragg spots corresponding to *P4/nmm* labeled is from the $LaOBiS_2$ single crystal. It can readily be seen that several Bragg spots (within the circle) are not reproduced

by this symmetry. Shown in Fig. 1C is the calculated pattern in color dots from *P4/nmm* that based on its reflection condition in the hk0 plane (h+k = 2n), odd combinations of h+k are forbidden. This is consistently observed in the superconducting crystal as well, as will be shown below. The integrated intensity of the neutron data across the $h\overline{3}0$ line is plotted in Fig. 1D. The forbidden reflections are much weaker by comparison to the main Bragg peaks. What is the underlying symmetry that can yield the right diffraction pattern?

To answer this question, we test previously proposed symmetries. The calculated diffraction patterns from four different symmetries are shown in Fig. 2. The corresponding unit cells are shown in the supporting Tables. *P4mm* and $P\overline{4}m2$ [8] are subgroups of *P4/nmm* (Fig. 2C and 2D). Given that the same reflection conditions apply as in the *P4/nmm*, neither symmetry can reproduce the new reflection conditions. In the $P2_1mn$ (Fig. 2B) symmetry suggested in Ref. [4], not all reflections can be reproduced by the calculated pattern either, because the reflection condition along the *h00* direction of h = 2n restricts the symmetry from producing extra reflections beyond the ones obtained in the *P4/nmm* symmetry. A final comparison with a fourth symmetry, $P2_1/m$, yields a Bragg structure with extra reflections as seen in Fig. 2A, but fails to reproduce critical reflections at spots marked in the figure. This leads us to conclude that the symmetry of $LaO_{1-x}F_xBiS_2$ is considerably lower than expected.

Of significance to the crystal structure is the motion of S1. Earlier results hinted at in-plane sulfur atom, S1, displacements possibly leading to ferroelectric like modes [4], although no structural transition was expected because of quantum zero-point motions that render the system dynamically disordered. Our earlier neutron powder diffraction measurements yielded a similar outcome but with a larger amplitude of displacement (about 0.3 Å [10]). Several displacement patterns can exist that can be either ferro-or antiferro-distortive in nature, in which the two S1 atoms in the BiS_2 bi-layers are displaced simultaneously in the x- or y-directions, either in parallel or anti-parallel. Distinction between the two patterns cannot be made from the powder data as each model results in the same magnitude of bonds regardless of orientation in real-space [10].

Within one unit cell, three unique directions of the S1 displacements are possible as listed here: (+x, +x), (+x, +y) and (+x, -x) where the two coordinates refer to the S1 ion in the bi-layers. Given that the lattice is nominally tetragonal and the a- and b-axes are equivalent, the magnitude of the displacement is the same in both directions, and the direction, either -x- or -y-, of the displaced ion can be altered. However, the displacement direction at one layer is important relative to the second layer. If the displacements are antiferro-distortive, the antiferro-distortive unit cell is doubled along the a- and b-axes (Fig. 3A). On the other hand, if the displacements are ferro-distortive, the ferro-distortive cell is not doubled (also shown in Fig. 3A). From the structure factor calculations, it is determined that when the displacement pattern is (+x, -x), no intensity is produced at Miller index h=0 when k is odd. When the displacement pattern is (x, x), the intensity is zero again when either h or k become odd. Thus the (+x, -x) and (+x, +x) patterns are excluded and not considered further.

Using the remaining pattern (+x, +y) (or equivalently (-x, -y)), the Bragg reflections in the *hk0* plane are calculated using the ferro- and antiferro-distortive modes in the *P1* symmetry. This pattern breaks the fourfold, twofold and inversion symmetry operations of the nominal *P4/nmm*. In Fig. 3B and 3C, the calculated reciprocal lattice patterns

corresponding to the two modes are shown. Far more reflections are observed in the antiferro-distortive mode, and can readily be eliminated when compared to the data from $LaOBiS_2$ (Fig. 1B) since it generates half integer peaks that are not actually present. On the other hand, the ferro-distortive mode can reproduce all Bragg spots. Thus the ferro-distortive mode remains as the only possibility.

To reproduce the Bragg peak intensity, a full profile refinement of the three dimensional neutron diffraction intensity is performed. This involves a total of about 4600 Bragg peaks. Several polytypes with different stacking distortion patterns along the c-axis are assumed. Four of them are shown in Fig. 4A. Each quadrant in a domain corresponds to a BiS_2 plane. Thus four quadrants correspond to four planes stacked along the c-axis where the layers are labeled as 1, 2, 3, and 4. Thus each domain represents an S1 distortion pattern in four consecutive planes. The displacement vector of the same magnitude designated by x or y are indicated with the arrows. The displacement pattern for the first domain is (-x, -y, -x, -y), for the second is (+x, +y, -x, -y), for the third is (-x, +y, -x, -y) and for the fourth is (-x, +x, -y, +y). The calculated structure factor for each displacement mode is compared to the observed structure function. All patterns produce a comparable agreement as determined from their χ^2 values (0.1414, 0.1373, 0.1408, 0.1383). At the same time, we find that when the calculated intensity from all Bragg peaks is averaged over all four domain structures, the fitting improves further and the result is shown in Fig. 3B with the χ^2. The plot between the observed and calculated squared intensities is on the expected line (blue line with a slope of 1), where the superlattice structure is well reproduced. Some differences are observed involving the highest intensity Bragg peaks. This suggests that all four domains are most likely present. Moreover, other displacement patterns are also likely, with different sequencing patterns, thus the four domain pattern presented here is just one solution to reproducing the peak intensity. It is nonetheless clear that the sulfur ferro-displacement is the key component to the broken crystal symmetry that can be significant in theoretical calculations.

To test the applicability of the model, the ferro-distortive cell is used to fit the data collected from the 30 % superconducting sample. Shown in Fig. 5A is the plot of the bulk magnetic susceptibility that shows a T_C ~2.5 K. The single crystals are not exposed to high pressure annealing as in the case of powders hence their T_C's are lower [2, 15]. At the same time, the stacking faults observed in the powder samples that are induced by the high-pressure treatment leading to a pronounced broadening of Bragg peaks with an l-component[14] are absent in single crystals. In Figs. 5B and 5C, it can readily be seen that the ferro-distortive mode can reproduce all Bragg reflections, just like in the parent compound. However, the magnitude of the x- and y-displacements of S1 is smaller, at 0.2 Å. A real-space arrangement of the four domains in the ab-plane can result in regions with varying degree of spatial uniformity that may not be conducive to superconductivity. When the domains are arranged along the c-axis, the experimental diffraction pattern is reproduced well which is consistent with the lattice accommodating many polytypes. However, the arrangement of the domains in the ab-plane is more critical because domain walls can be created which are antiferro-distortive. These can give rise to additional peaks not present in the data as can be seen from the diffraction pattern in Fig. 5E of the two-dimensional arrangement shown in Fig. 5D. Thus, lattice uniformity is important in the ab-plane, but the polytypes can alternate along the c-axis. Charge carriers can get trapped in the lattice deformations reducing the

effective number of carriers available for pairing.

The electronic structure and Fermi surface of $LaOBiS_2$ resemble that of superconducting MgB_2 although T_C is much higher in the latter [18, 19, 20]. Even though their coupling constants are comparable, T_C is significantly lower in the current system because the main contribution stems from low frequency phonon modes [8]. Can the proposed displacement mode lead to charge disproportionation, ferroelectricity in Bi or a charge density wave (CDW)? In the $BaBiO_3$ phonon superconductor, the Bi-O bonds are split at 2.11 and 2.29 Å [21] due to a breathing [11] or a Peierls-like[22] instability. However, with K doping as in $Ba_{0.6}K_{0.4}BiO_3$, the split disappears and the bond lengths become one, 2.14 Å [23, 24], which is not the case in the superconducting $LaO_{0.7}F_{0.3}BiS_2$ in which the distortions are present, albeit reduced in magnitude. In conclusion, the structure of $LaO_{1-x}F_xBiS_2$ is exposed. The sulfur mode that can explain the single crystal results is ferro-distortive in nature, and must be responsible for the large electron-phonon coupling. This mode must bring significant changes in the electronic structure around the Fermi level. Fluctuations of the bond lengths in the superconducting crystal as shown here indicate that charge fluctuations persist and are most likely significant in the mechanism of superconductivity. Thus the electronic pairing and the form of superconductivity present in this system is sensitive to the precise nature of the crystal structure.

Acknowledgments

The authors would like to acknowledge support from the National Science Foundation, DMR-1404994, 1265162 and 1334170. Work at ORNL was supported by the US Department of Energy, Office of Basic Energy Sciences, Materials Sciences and Engineering Division and Scientific User Facilities Division. Work at the Advanced Photon Source, was supported by the US Department of Energy, Office of Science User Facility, and operated by Argonne National Laboratory under Contract No. DE-AC02-06CH11357.

References

[1] Mizuguchi, Y., Fujihasa, H., Gotoh, Y., Suzuki, K., Usui, H., Kuroki, K., Demura, S., Takano, Y., Izawa, H. and Miura O., *BiS_2-based layered superconductor $Bi_4O_4S_3$*, Phys. Rev. B 86 (2012), pp. 220510(R).

[2] Mizuguchi, Y., Demura, S., Deguchi, K., Takano, Y., Fujihasa, H., Gotoh, Y., Izawa, H. and Miura O., *Superconductivity in Novel BiS_2-Based Layered Superconductor $LaO_{1-x}F_xBiS_2$*, J. Phys. Soc. Jpn. 81, (2012), pp. 114725.

[3] Usui, H., Suzuki, K. and Kuroki, K., *Minimal electronic models for superconducting BiS_2 layers*, Phys. Rev. B 86 (2012), pp.220501(R).

[4] Yildirim, T., *Ferroelectric soft phonons, charge density wave instability, and strong electron-phonon coupling in BiS_2 layered superconductors: A first-principles study*, Phys. Rev. B 87 (2013), pp. 020506(R).

[5] Wan, X., Ding, H.-C., Savrasov, S. Y. and Duan, C.-G., *Electron-phonon superconductivity near charge-density-wave instability in $LaO_{0.5}F_{0.5}BiS_2$: Density-functional calculations*, Phys. Rev. B 87 (2013), pp. 115124.

[6] Orenstein, J. and Millis, A. J., *Advances in the Physics of High-Temperature Superconductivity*, Science 288 (2000), pp. 468-474.

[7] Liu, Q., Zhang, X., Jin, H., Lam, K., Im, J., Freeman, A. J. and Zunger, A., *Search and design of nonmagnetic centrosymmetric layered crystals with large local spin polarization*, Phys. Rev. B 91 (2015), pp. 235204.

[8] Li, B., Xing, Z. W. and Huang, G. Q., *Phonon spectra and superconductivity of the BiS2-based compounds $LaO_{1-x}F_xBiS_2$*, Euro. Phys. Lett. 101 (2013), pp. 47002.

[9] Mizuguchi, Y., *Superconductivity in BiS_2-Based Layered Compounds*, Phys. Procedia 58 (2014), pp. 94-97.

[10] Athauda, A., Yang, J., Lee, S.-H., Mizuguchi, Y., Deguchi, K., Takano, Y., Miura, O. and Louca, D., *In-plane charge fluctuations in bismuth-sulfide superconductors*, Phys. Rev. B 91 (2015), pp. 144112.

[11] Mazin, I. I., Liechtenstein, A. I. and Ivanov, O. V., *Breathing instability and disproportionation of Bi^{4+} ions in $BaBiO_3$*, Ferroelectrics 164 (1995), pp. 169-175.

[12] Sheldrick, G. M., *A short history of SHELX*, Acta Crystal. A64 (2008) pp.112-122.

[13] Yazici, D., Huang, K., White, B. D., Chang, A. H., Friedman, A. J., and Maple, M. B., *Superconductivity of F-substituted $LnOBiS_2$ (Ln=La, Ce, Pr, Nd, Yb) compounds*, Phil. Mag. 93 (2013), pp. 673.

[14] Lee, J., Stone, M. B., Huq, A., Yildrim, T., Ehlers, G., Mizuguchi, Y., Miura, O., Takano, Y., Deguchi, K., Demura, S. and Lee, S.-H., *Crystal structure, lattice vibrations, and superconductivity of $LaO_{1-x}F_xBiS_2$*, Phys. Rev. B 87 (2013), pp. 205134.

[15] Kajitani, J., Deguchi, K., Omachi, A., Hiroi, T., Takano, Y., Takatsu, H., Kadowaki, H., Miura, O. and Mizuguchi Y., *Correlation between crystal structure and superconductivity in $LaO_{0.5}F_{0.5}BiS_2$*, Solid State Commun. 181 (2014), pp. 1-4.

[16] Miura, A., Nagao, M., Takei, T., Watauchi, S., Tanaka, I. and Kumada, N., *Crystal structures of $LaO_{1-x}F_xBiS_2$ (x0.23, 0.46): Effect of F doping on distortion of Bi?S plane*, J. Solid State Chem. 212 (2014), pp. 213-217.

[17] Lei, H., Wang, K., Abeykoon, M., Bozin, E. S. and Petrovic, C., *New Layered Fluorosulfide $SrFBiS_2$*, Inorg. Chem. 52 (18) (2013), pp. 10685-10689.

[18] Kong Y., Dolgov O. V., Jepsen O., and Andersen, O. K., *Electron-phonon interaction in the normal and superconducting states of MgB_2*, Phys. Rev. B 64 (2001), pp. 020501.

[19] Kortus J., Mazin I. I., Belashchenko K. D., Antropov V. P. and Boyer L. L., *Superconductivity of Metallic Boron in MgB_2*, Phys. Rev. Lett. 86 (2001), pp. 4656-4659.

[20] Nagamatsu, J., Nakagawa, N. Muranaka, T., Zenitani, Y. and Akimitsu, J., *Superconductivity at 39 K in magnesium diboride*, Nature (London) 410 (2001), pp. 63-64.

[21] Hinks, D. G., Dabrowski, B., Jorgensen, J. D., Mitchell, A. W., Richards, D. R., Pei, S. and Shi, D., *Synthesis, structure and superconductivity in the* $Ba_{1-x}K_xBiO_{3-y}$ *system*, Nature 333 (1988), pp. 836-838.

[22] Mattheiss, L. F., Gyorgy, E. M. and Johnson, D. W., Jr., *Superconductivity above 20 K in the Ba-K-Bi-O system*, Phys. Rev. B 37 (1988), pp. 3745(R).

[23] Heald, S. M., DiMarzio, D., Croft, M., Hegde, M. S., Li, S. and Greenblatt, M., *X-ray-absorption study of charge-density ordering in* $(Ba_{1-x}K_x)BiO_3$, Phys. Rev. B 40 (1989), pp. 8828.

[24] Salem-Sugui, S., Jr., Alp, E. E., Mini, S. M., Ramanathan, M., Campuzano, J. C., Jennings, G., Faiz, M., Pei, S., Dabrowski, B., Zheng, Y., Richards, D. R. and Hinks, D. G., *Determination of the local structure in* $Ba_{1-x}K_xBiO_3$ *by x-ray-absorption spectroscopy*, Phys. Rev. B 43 (1991), pp. 5511.

[25] Sagayama R., Sagayama H., Kumai R., Murakami Y., Asano T, Kajitani J., Higashinaka R., Matsuda T. D. and Aoki Y., *Symmetry Lowering in* $LaOBiS_2$*: A Mother Material for* BiS_2*-Based Layered Superconductors*, J. Phys. Soc. Jpn. 84, (2015), pp. 123703.

[26] Athauda A., Yang J., Li B., Mizuguchi Y., Lee S.-H., and D. Louca, *The Crystal Structure of Superconducting* $LaO_{1-x}F_xBiS_2$, J. Supercond. Nov. Magn. 28, (2015), pp. 1255-1259.

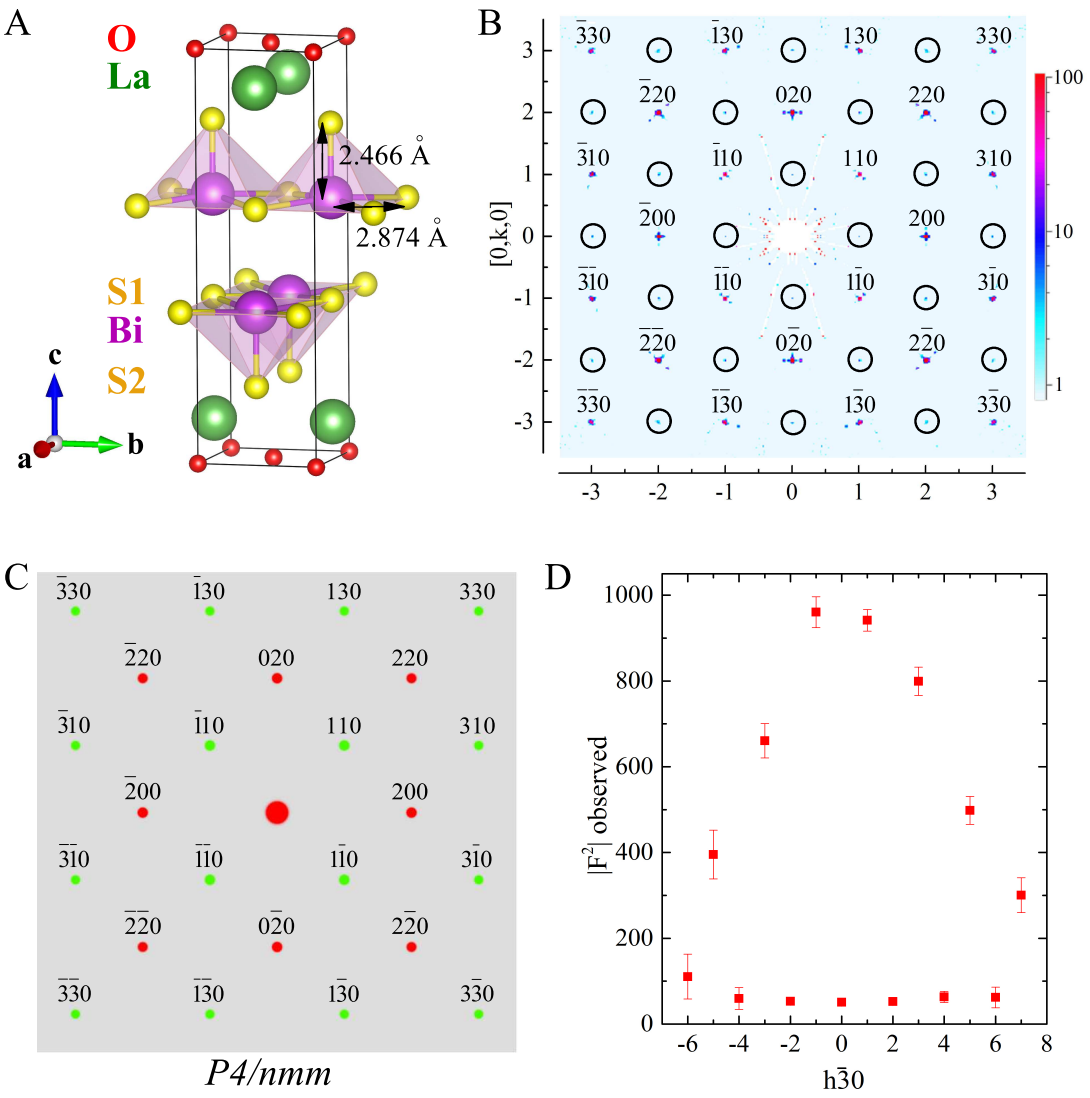

Figure 1: In A, the layer crystal structure with the Bi-bilayer is shown. In B, the single crystal neutron diffraction pattern (black dots) in the hk0 reciprocal plane for the parent compound, LaOBiS2, is shown. Several additional reflections are observed as circled. In C, the *hk0* plane is constructed using the *P4/nmm* symmetry. In D, the integrated intensity of the observed peaks is plotted along the h$\bar{3}$0 line.

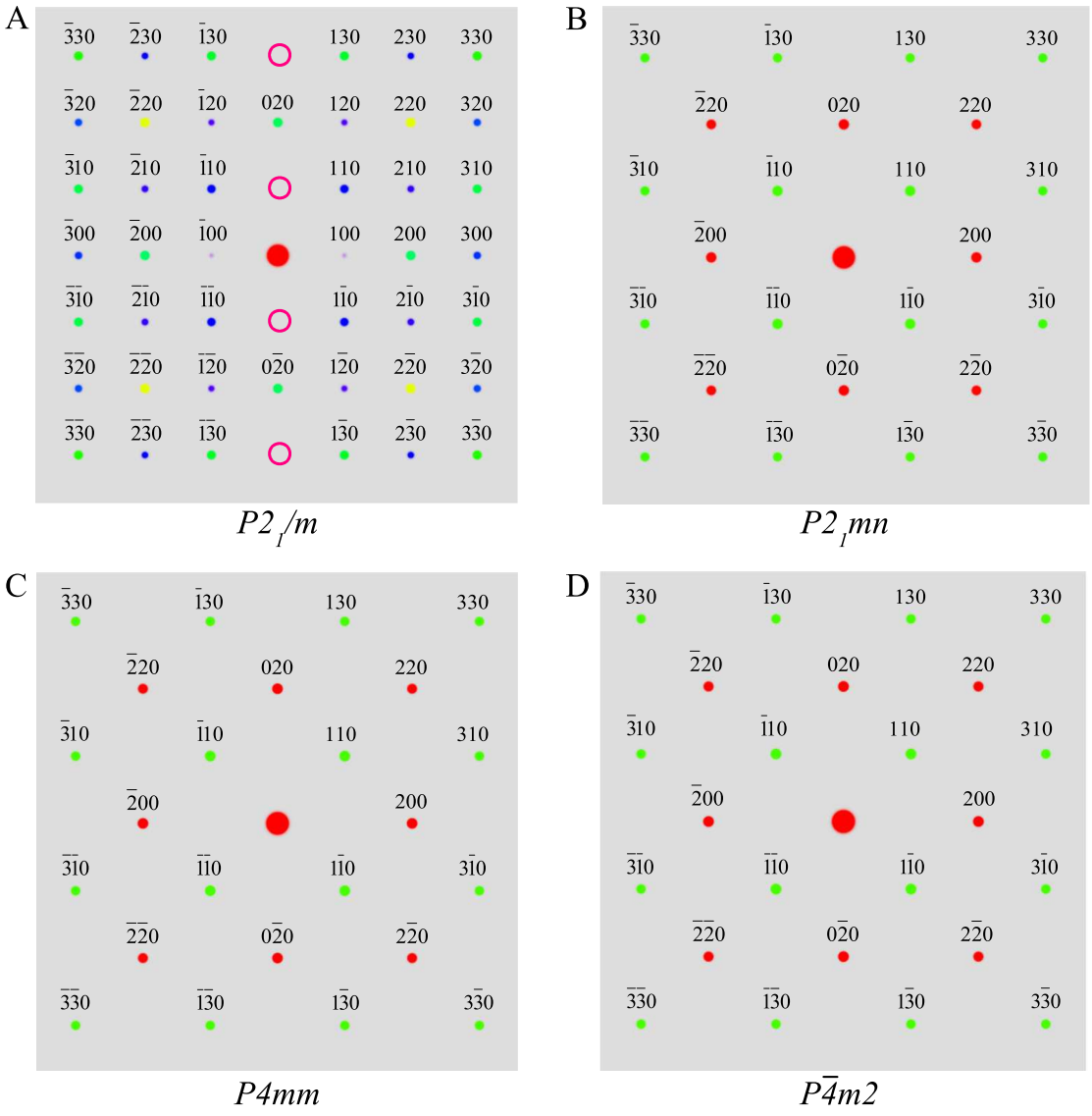

Figure 2: In A through D, the calculated reciprocal lattice patterns based on the four symmetries.

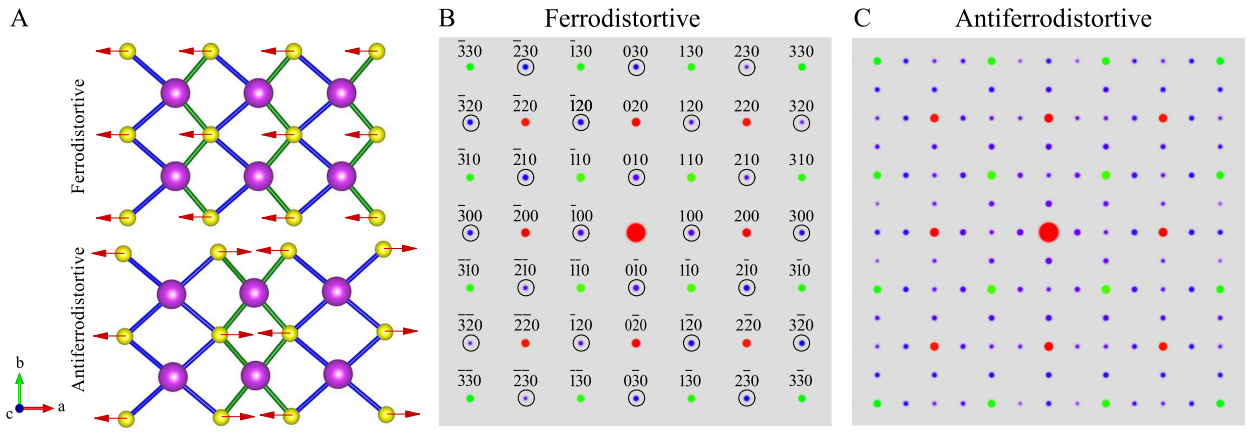

Figure 3: The ferro-distortive and anti-ferrodistortive displacements modes are shown in A. Only in-plane S1 atoms are allowed to move. In B, the calculated diffraction pattern from the ferro-distortive mode is shown while in C, the diffraction pattern resulting from the antiferro-distortive mode is shown.

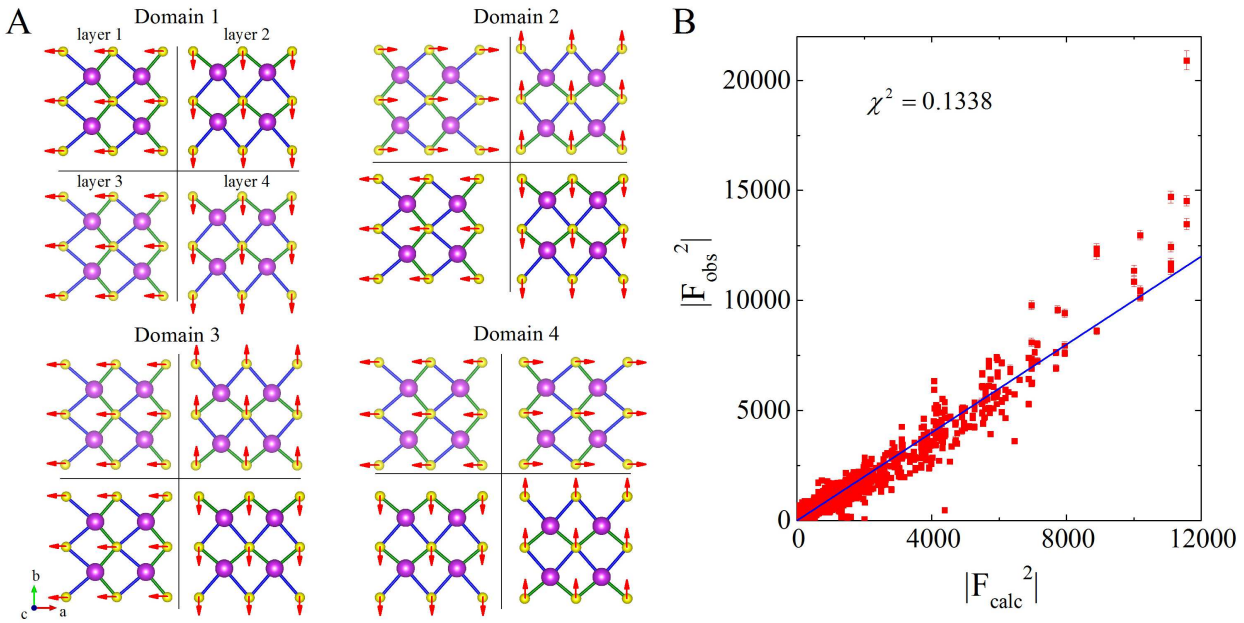

Figure 4: In A, four domain structures corresponding to displacements of S1 along the c-axis are shown. Each domain contains four quadrants where each quadrant represents one BiS_2 layer along the c-axis. In B, the square of the structure function, |F(Q)|2, for the observed intensity is compared to the calculated intensity obtained from the refinement based on averaging over all four domains. The fitting is done using the neutron single crystal data. The goodness of fit is determined to be 0.133. The blue line represents the ideal match between the calculated and the observed value at each Bragg peak with a slope of 1. Deviations are observed for the highest intensity peaks.

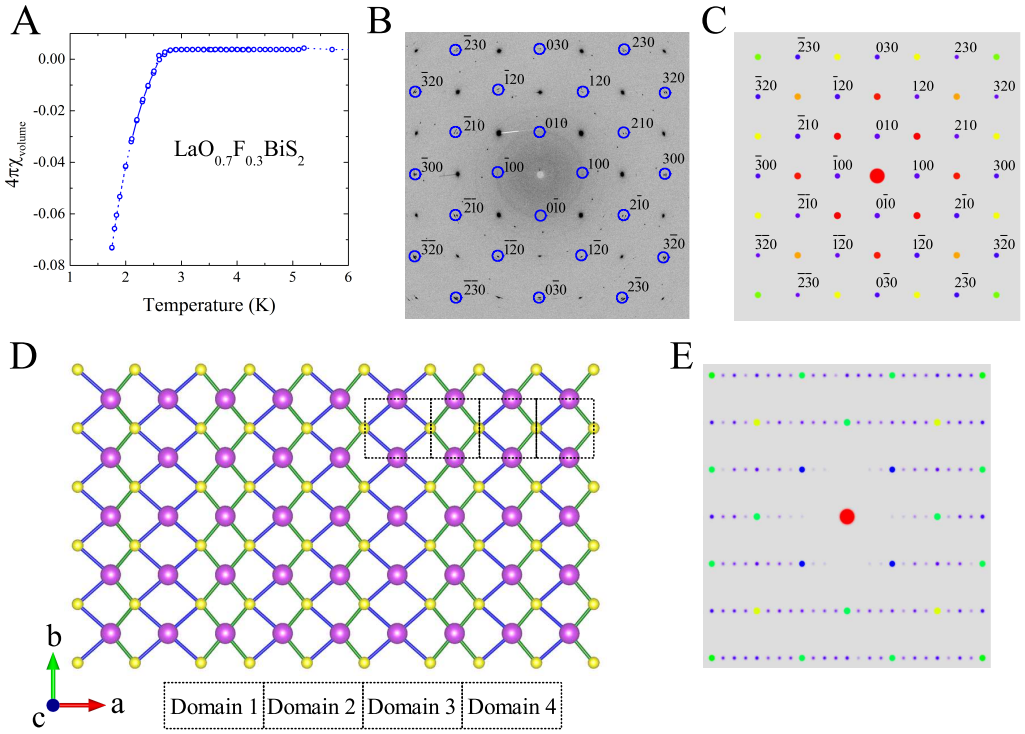

Figure 5: In A, the bulk magnetic susceptibility of the x = 0.3 crystal is shown. In B and C, the X-ray data in the *hk0* plane and the calculated pattern assuming the ferro-distortive pattern are shown. In D, an example is shown in which the domains are arranged in the ab-plane. Domain walls appear at the interfaces when the distortions change orientation and give rise to antiferro-distortive displacements. Shown in E is the calculated pattern from the real-space arrangement shown in D. Extra reflections are produced from this model that do not match the pattern shown in B.

Supporting Information

Table S1: The tested model of $P2_1/m$ [25] symmetry

$LaOBiS_2$	$P2_1/m$ (#11)		
	a(Å)	4.0769	
	b(Å)	4.0618	
	c(Å)	13.885	
	β(°)	90.12	
	x	y	z
La	0.2496	0.25	0.0899
Bi	0.2346	0.25	0.6309
S1	0.219	0.25	0.3844
S2	0.2483	0.25	0.8094
O	0.753	0.25	0.002

Table S2: The tested model of $P2_1mn$ [4] symmetry

$LaOBiS_2$	$P2_1mn$ (#31)		
	a(Å)	4.037	
	b(Å)	4.029	
	c(Å)	14.217	
	x	y	z
La	0.4997	0	0.0858
Bi	0.4973	0	0.6324
S1	0.525	0	0.3946
S2	0.4988	0	0.8102
O	0.4996	0.5	0

Table S3: The tested model of P4mm symmetry

$LaOBiS_2$	P4mm (#99)		
	a(Å)	4.0544	
	b(Å)	13.8246	
	x	y	z
La	0	0	0.0904
La	0.5	0.5	0.9096
Bi	0	0	0.6312
Bi	0.5	0.5	0.3688
S1	0	0	0.3832
S1	0.5	0.5	0.6168
S2	0	0	0.8096
S2	0.5	0.5	0.1904
O	0.5	0	0

Table S4: The tested model of $P\bar{4}m2$ [8] symmetry

$LaOBiS_2$	$P\bar{4}m2$ (#115)		
	a(Å)	4.1091	
	b(Å)	13.4196	
	x	y	z
La	0.5	0	0.1073
Bi	0	0.5	0.3855
S1	0.5	0	0.3844
S2	0.5	0	0.8128
O	0	0	0
O	0.5	0.5	0

Table S5: The tested model of P4/nmm [26] symmetry

$LaOBiS_2$	P4/nmm (#129)		
	a(Å)	4.0544	
	b(Å)	13.8246	
	x	y	z
La	0.5	0	0.0904
Bi	0	0.5	0.3688
S1	0.5	0	0.3832
S2	0.5	0	0.8096
O	0	0	0